Thermochimica Acta 477 (2008) 42–47

Contents lists available at ScienceDirect

Thermochimica Acta

journal homepage: www.elsevier.com/locate/tca

Effect of mixed ternary transition metal ferrite nanocrystallites on thermal decomposition of ammmonium perchlorate☆

Gurdip Singh[a,*], I.P.S. Kapoor[a], Shalini Dubey[a], Prem Felix Siril[b], Jian Hua Yi[c], Feng-Qi Zhao[c], Rong-Zu Hu[c]

[a] Chemistry Department, D.D.U. Gorakhpur University, Gorakhpur 273009, India
[b] University of Hudderfield, Hudderfield HD1 3DH, UK
[c] National Key Laboratory Xi_an Morden Chemistry Research Institute, Xi_an 710065, PR China

ARTICLE INFO

Article history:
Received 12 April 2008
Received in revised form 11 August 2008
Accepted 12 August 2008
Available online 26 August 2008

Keywords:
Mixed ternary transition metal ferrite (MTTMF) nanocrystallites
Ammonium perchlorate (AP)
Catalytic activity
Thermal decomposition
IR
BET equation

ABSTRACT

Nanocrystallites of six mixed ternary transition metal ferrite (MTTMF) were prepared by co-precipitation method and characterized by X-ray diffraction (XRD) and BET equation. XRD patterns gave average particle size for $NiZnFe_2O_4$ (NZF), $CuCoFe_2O_4$ (CuCoF), $NiCuFe_2O_4$ (NCuF), $CuZnFe_2O_4$ (CuZF), $CoNiFe_2O_4$ (CoNF) and $CoZnFe_2O_4$ (CoZF) as 7.2, 3.0, 3.0, 6.8, 3.9 and 5.8 nm, respectively. Further, catalytic activities of the MTTMF nanocrystallites on thermal decomposition of ammonium perchlorate (AP) were investigated using thermogravimetric analysis (TG), differential scanning calorimetry (DSC), differential thermal analysis (DTA), and ignition delay measurements. IR-active internal mode of cation and anion of ammonium perchlorate changes with temperature in presence of MTTMF nanocrystallites. The catalytic activity was found to be in the order: CoZF > CoNF > CuZF > CuCoF > NCuF > NZF. Nanocrystals of MTTMF have been proposed to play a significant role in the decomposition of AP.

1. Introduction

Spinel oxides (ferrospinels or ferrites) are of considerable interest due to their diverse applications in optical, electronic, catalytic, magnetic materials, etc. [1]. The ferrospinel of general formula $M^{2+}[Fe^{3+}]O_4{}^{2-}$ having ferric ion in square bracket occupies octahedral position and metal ion outside the bracket occupy tetrahedral site. M^{2+} represents the divalent ion such as Mn^{2+}, Zn^{2+}, Co^{2+}, Cu^{2+}, Ni^{2+}, etc. Ferrite spinels may also contain mixture of two divalent metal ions, in which ratio of these divalent metal ions may vary, are called mixed ferrite. The cations distribution of mixed ferrite significantly affects the surface properties of ferrospinels making them catalytically active. Because of their small size and large number of cations, for co-ordination sites, nanocrystallites are capable of enhancing the rate of chemical reactions and are increasingly gaining popularity as reactive nanocrystallites.

The synthesis of nanocrystallites was achieved by the co-precipitation of sparingly soluble products from aqueous solution followed by thermal decomposition of these products to oxides. Co-precipitation reaction involves the simultaneous occurrence of nucleation, growth, coarsening and/or agglomeration processes. The co-precipitate is then calcined at low temperatures (300 °C) [2,3] as sintering occurs at high temperature leading to coarse particles.

The catalytic activity of transition metal oxides are studied in the thermal decomposition of AP [4–7] which is used as an oxidizer in composite solid propellants (CSPs). The transition metal oxides are also used as burning rate modifiers for CSPs [8–10]. In our previous paper of nanomaterials, we have reported that when the size of the oxide reduced to nanometer scale, catalytic activity of transition metal oxides (TMOs) increases many fold [11]. Thus the preparation, characterization and catalytic activity of mixed ternary transition metal ferrites (MTTMFs) on the thermal decomposition of AP are described here.

2. Experimental

2.1. Materials

AP obtained from Centre Electrochemical Research Institute (CECRI), Karaikudi, was used as such without further purification.

☆ Part 61.

* Corresponding author. Tel.: +91 551 2202856; fax: +91 551 2340459.
E-mail address: gsingh4us@yahoo.com (G. Singh).

0040-6031/$ – see front matter © 2008 Elsevier B.V. All rights reserved.
doi:10.1016/j.tca.2008.08.005

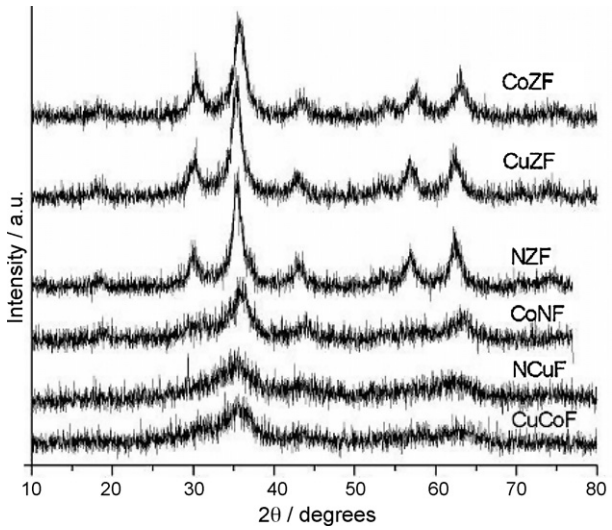

Fig. 1. XRD patterns of ferrite nanocrystallites. Short names of the nanocrystallites are marked in the figure.

Crystals of AP were ground into fine powder using a pestle and mortar and sieved to 100–200 mesh. Nitrates of Cu, Ni, Zn, and Fe(III) of Merck Limited, Mumbai; Co nitrate of Qualigens Fine Chemicals, Mumbai and NaOH of Merck Limited, Mumbai were used as received.

2.2. Preparation of MTTMF nanocrystallites

All ferrospinels were prepared by co-precipitation method as reported earlier [12]. An aqueous solution of the mixed nitrate was prepared initially in the required molar proportion. Drop-wise addition of N/2 NaOH solution with vigorous stirring gave complete precipitate of metal hydroxides in the pH range 11–12. The precipitates of mixed hydroxides were washed with distilled water to make them free from nitrate ions; kept at 60 °C in a hot air oven for 24 h and dried. They were calcined at 300 °C for about 5 h [12]. In our experiment, we find that at 300 ± 10 °C, brown colored metal hydroxides could change to black colored MTTMF nanocrystallite.

2.3. Characterization

XRD measurements were performed on the ferrospinel nanocrystallites by X-ray diffractometer using CuKα radiation (λ = 1.5418 Å). The diffraction patterns are shown in Fig. 1. Particle size of the crystallites was calculated by applying Scherrer's formula [13,14] to the powder XRD data and the values are reported in Table 1. Surface area, pore volume and pore size were measured by N_2 porosimetry using a Micrometrics ASAP 2020 instrument. All the catalysts were degassed at 250 °C, then N_2 adsorption and desorption were done and isotherms were recorded at −196 °C. Surface area was calculated using BET equation. Adsorption data were used to calculate the pore volume and diameter using BJH equation. The results of nitrogen porosimetry are reported in Table 1.

2.4. IR studies

The coupled simultaneous technique of in-situ thermolysis cell (Amoy University Instrument Co., China) with rapid-scan Fourier transform infrared spectroscopy (Nicolet 60SXR Co., USA) (thermolysis/RSFT-IR) was employed to explore the mechanism of thermolysis. The thermolysis cell heating rate, 10 K min^{-1} and atmosphere, air. Solid thermolysis spectra acquisition rate, 7.48 files mm^{-1}; resolution, 4 cm^{-1} and using a DTGS detector. Gas thermolysis probe heated up to 700 °C for T-Jump/RSFT-IR test at heating rate of 700 K s^{-1}, and maintained for 10 s; spectra acquisition rate, 5 files s^{-1}; resolution, 4 cm^{-1} and a MCT–A rapid-scan IR detector which fixed several millimeters above the sample surface; sample mass, ~1 mg.

Table 1
Crystallite size, surface area, pore volume and pore size of MTTMF nanocrystallites by nitrogen porosimetry

Sample	Crystal size[a] (nm)	Surface area[b] ($m^2 g^{-1}$)	Pore volume[c] ($cm^3 g^{-1}$)	Pore size[d] (nm)
NZF	7.2	108.2	0.17	4.98
CuCoF	3.0	134.0	0.20	4.87
NCuF	3.0	99.5	0.15	4.48
CuZF	6.8	92.0	0.12	4.27
CoNF	3.9	104.2	0.17	5.26
CoZF	5.8	62.2	0.09	4.82

[a] Calculated using the Scherrer's formula on the diffraction peak of maximum intensity.
[b] From BET equation.
[c] Total volume of pores using BJH equation during adsorption.
[d] From BJH equation during adsorption.

2.5. Catalytic activity measurements on thermolysis of AP

Catalytic activities of the prepared ferrospinel nanocrystallites on thermolysis of AP were studied using a number of thermoanalytical techniques such as non-isothermal and isothermal TG, DTG, DSC, DTA and ignition delay (D_i) measurements after mixing 1% of MTTMF nanocrystallites with AP.

2.5.1. Non-isothermal TG

TG studies on pure AP and AP with these MTTMF nanocrystallites (by mixing in ratio of 99:1) were undertaken in static air atmosphere at a heating rate 10 K min^{-1} using indigenously fabricated apparatus [15]. Gold crucible was used as sample holder. The thermograms of mass loss % vs. temperature (°C) are reported in Fig. 2.

2.5.2. Simultaneous TG–DTG and DSC

TG–DTG and DSC curves (Figs. 3 and 4) under flowing nitrogen gas (purity 99.99%, flowing rate 60 cm^3 min^{-1}; atmospheric pres-

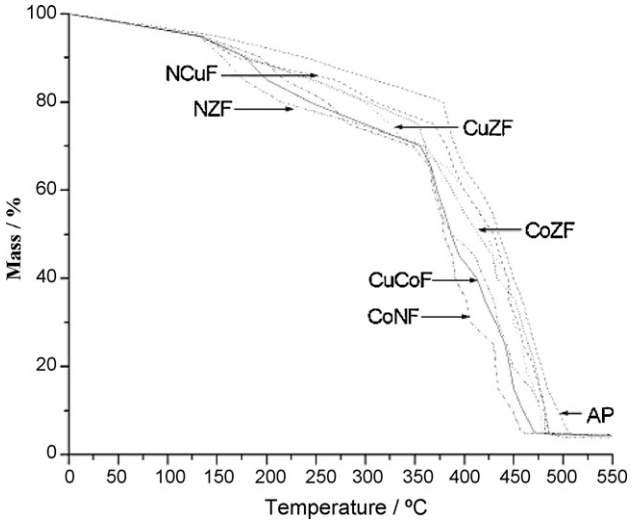

Fig. 2. Non-isothermal TG thermal curves of AP and the MTTMF nanocrystallites (1% by mass) at 10 °C min^{-1} under static air atmosphere.

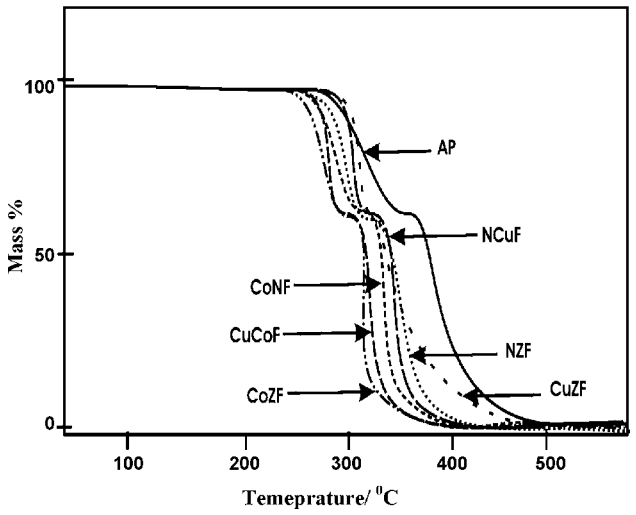

Fig. 3. Non-isothermal TG thermal curves of AP and the MTTMF nanocrystallites (1% by mass) at 10 K min^{-1} under N_2 atmosphere.

sure) were obtained by using a TA2950 thermal analyzer (TA Co., USA) and TA910S differential scanning calorimeter (TA Co., USA) respectively. The conditions of TG–DTG analysis were as follows: sample mass, ~0.5 mg; heating rate, 10 K min^{-1} and for the DSC analysis, using crucible with pierced lid, sample mass, ~0.5 mg; heating rate, 10 °C min^{-1}.

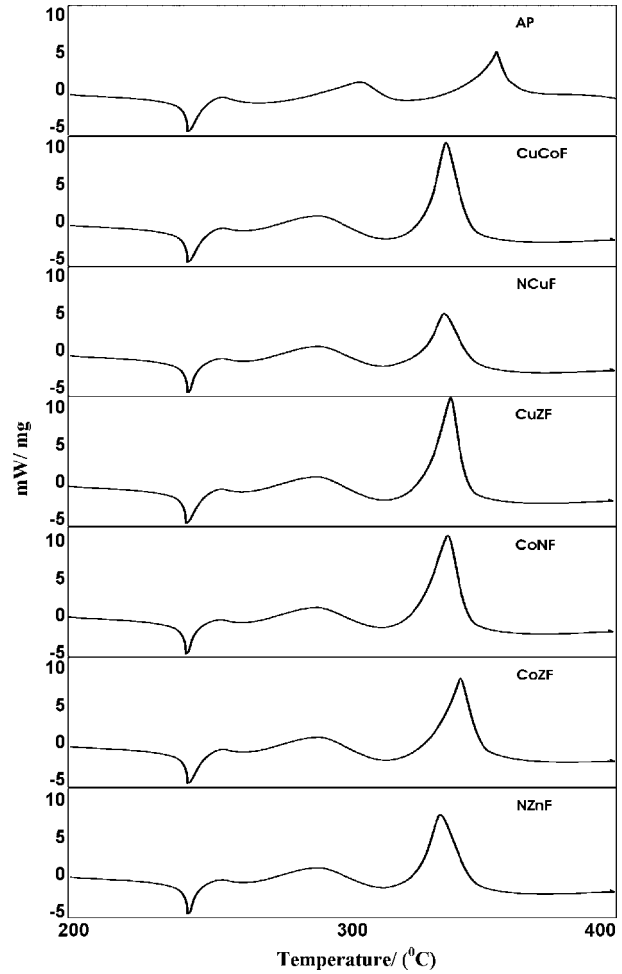

Fig. 4. DSC thermal curves of AP and the MTTMF nanocrystallites (1% by mass) on the pans with pierced lid, at 10 K min^{-1} under N_2 atmosphere.

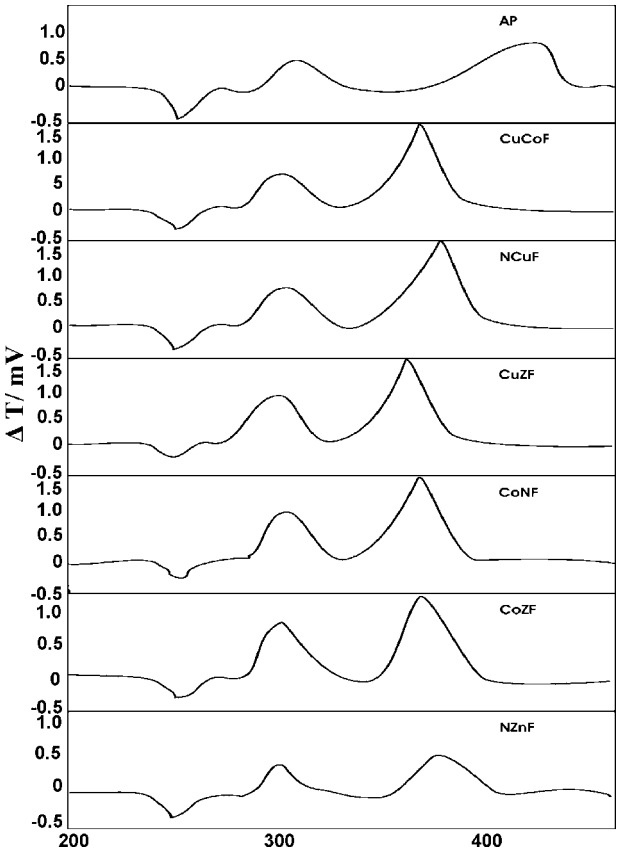

Fig. 5. DTA thermal curves of mixtures of AP and the MTTMF nanocrystallites (1% by mass) at 10 K min^{-1} under static air atmosphere.

2.5.3. DTA

DTA thermal curves (Fig. 5) recorded on Universal Thermal Analysis Instrument, Mumbai, under static air atmosphere on 20 mg samples were recorded at 10 K min^{-1} heating rate.

2.5.4. Isothermal TG

Isothermal TG thermal curves (Fig. 6) were also recorded on AP and its mixtures with the MTTMF nanocrystallites of varying compositions (0.25, 0.5, 1 and 2% by mass) at 280 °C under static air atmosphere.

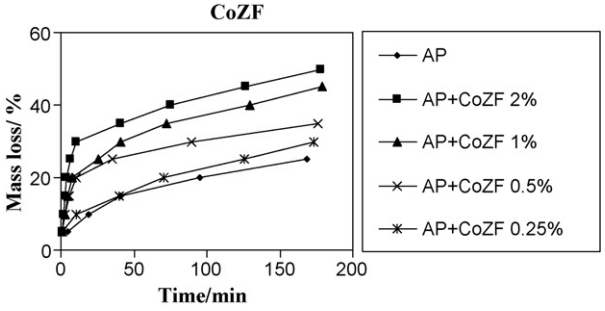

Fig. 6. Isothermal TG of various % of CoZF nanocrysallites in AP at 280 °C, same result found for rest of MTTMF nanocrystallites.

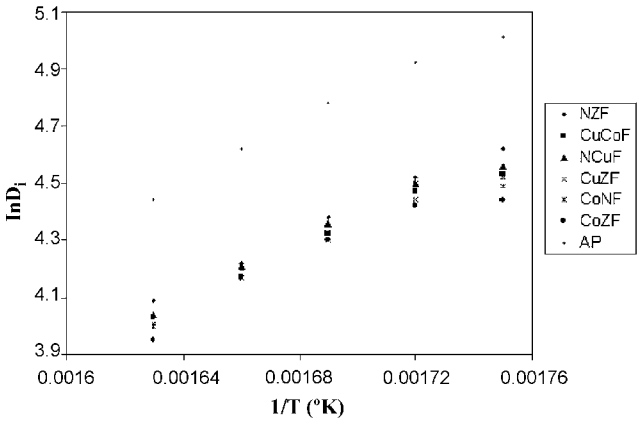

Fig. 7. Plots of $\ln D_i$ vs. $1/T$ for 1% of MTTMF nanocrysallites in AP.

2.5.5. Ignition delay

This measurement was undertaken using the tube furnace (TF) technique [16] in the temperature range of 300–340 °C. 20 mg of samples (pure AP and AP with MTTMF nanocrystallites in same ratio as in TG) were taken in an ignition tube and time intervals (determined with help of stop watch) between the insertion of the ignition tube into the TF and the moment of ignition indicated by the appearance of fumes with light, gave the value of ignition delay in seconds. The sample was inserted into the TF with the help of a bent wire. The time for the insertion of the ignition tube into the TF was kept constant throughout each run. The accuracy of temperature measurements of TF was ±1 °C. Each run was taken five times and mean D_i values are reported in Table 4. The D_i data were found to fit in the Eq. (1) [17–19].

$$D_i = A \exp\left(\frac{E_a}{RT}\right) \quad (1)$$

where E_a is activation energy for thermal explosion, A is the pre-exponential factor, and T the absolute temperature. E_as assessed by Eq. (1) along with the correlation coefficients (r) are given in Table 4 and the plots of $\ln D_i$ vs. $1/T$ are presented in Fig. 7.

3. Results and discussion

The XRD patterns (Fig. 1) for all these MTTMF nanocrystallites show considerable broadening of the peaks, which is due to the presence of very small crystallites. When such peak broadening is observed in XRD patterns, size of the crystallites can be calculated by applying Scherrer's formula. Size of these very small crystallites (Table 1) shows beyond doubt that the prepared ferrospinels are in the nanometer range. Nitrogen porosimetry data showed that the nanocrystallites have considerably high surface area and pores volume. Among ferrites, CuCoF has the highest surface area whereas CoZF has the lowest. The rest of MTTMF have almost similar surface areas. Pore volume of these nanocrystallites follows same order as the surface area. This indicates that the nanocrystallites do exist as aggregates and the measured pore characteristics are the features of intercrystalline voids.

The non-isothermal TG curves in static air (Fig. 2) and in flowing N_2 atmosphere (Fig. 3) for pure AP, clearly indicate that thermal decomposition of AP takes place in two steps [20–22], TG thermal curves (Figs. 2 and 3) for AP with ferrites do confirm that the catalysts affect both LTD and HTD processes and further gasification of AP in presence of catalyst during HTD process not only begins early but also complete at lower temperature (30–60 °C). It is inferred that the temperature difference observed under static air and inert atmosphere is due to experimental conditions. DTG peaks also confirm lowering temperature of HTD (Table 2).

DSC and DTA thermal curves (Figs. 4 and 5) for the decomposition of pure AP show three events. The endothermic peak in DTA at 245 °C and in DSC at 246 °C represents the transition of AP from orthorhombic to cubic [11]. The temperature difference observed for HTD peak temperature may be due to different experimental conditions. DSC and DTA thermal curves of AP in presence of MTTMF nanocrystallites showed noticeable change in the decomposition pattern (Table 2).

Table 3
Decomposition rate and catalytic activity of AP and AP + MTTMF nanocrystallites

Sample	Decomposition rate (for 25%decomposition, min^{-1}) of MTTF nanocrystallites	Catalytic activity (C_A)
AP	0.142	–
AP + NZF	0.451	3.2
AP + CuCoF	0.641	4.5
AP + NCuF	0.556	3.9
AP + CuZF	0.814	5.7
AP + CoNF	0.893	6.3
AP + CoZF	0.977	6.9

Table 2
DTG, DSC and DTA phenomenological data of the AP and AP with ferrite nanocrystallites

Samples	DTG		DSC		DTA	
	Peak temperature (°C)	Nature	Peak temperature (°C)	Nature	Peak temperature (°C)	Nature
AP	300	Exo	300	Exo	305	Exo
	370	Exo	358	Exo	443	Exo
NZF	295	Exo	285	Exo	300	Exo
	342	Exo	338	Exo	370	Exo
CoNF	295	Exo	283	Exo	295	Exo
	340	Exo	331	Exo	370	Exo
CoZF	295	Exo	283	Exo	295	Exo
	340	Exo	336	Exo	365	Exo
CuCoF	295	Exo	285	Exo	300	Exo
	344	Exo	338	Exo	365	Exo
CuZF	295	Exo	287	Exo	295	Exo
	341	Exo	330	Exo	365	Exo
NCuF	295	Exo	282	Exo	295	Exo
	342	Exo	322	Exo	370	Exo

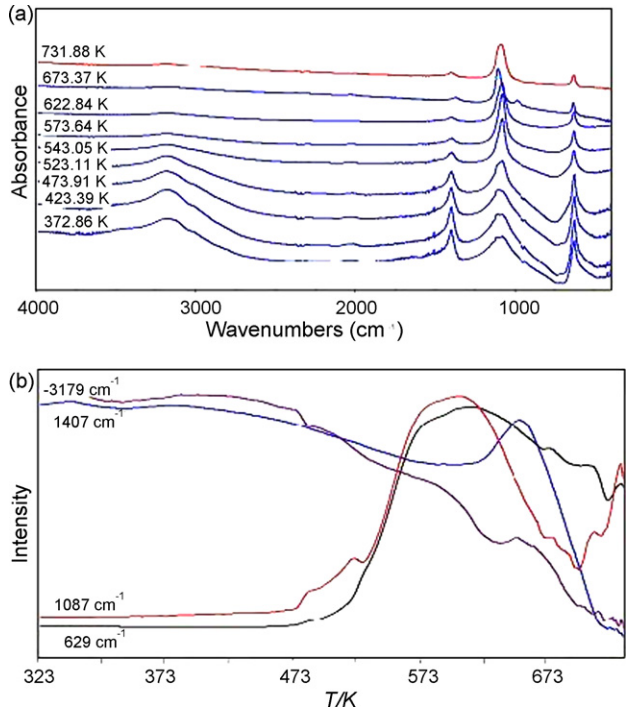

Fig. 8. (a) IR spectra of the condensed phase decomposition products of the pure AP at various temperatures and (b) IR characteristics absorption peak intensity of the condensed phase decomposition products of pure AP at various temperatures.

The catalytic activities of these ferrites i.e. the rates of decomposition at 25% mass loss of AP and its mixtures with the MTTMF nanocrystallites have been calculated from isothermal TG curve shown in Fig. 6 and the values are given in Table 3. The catalytic activity (C_A) of these catalysts has been estimated by using following equation:

$$\text{catalytic activity}\,(C_A) = \frac{C_0}{C}$$

where C_0 is rate of decomposition of catalyzed AP and C is rate of decomposition of pure AP.

It has been observed (Fig. 6, Table 3) that MTTMF nanocrystallites were found to enhance the thermal decomposition of AP to a greater extent. It is inferred that this fact could be due to nanosize of the ferrites. The order of catalytic activity of MTTMF nanocrystallites on AP thermal decomposition from Table 3 seems to be

CoZF > CoNF > CuZF > CuCoF > NCuF > NZF

The catalytic activity was found to be increased with increasing amount of the catalysts. Similar results were obtained from all six ferrite nanocrytallites.

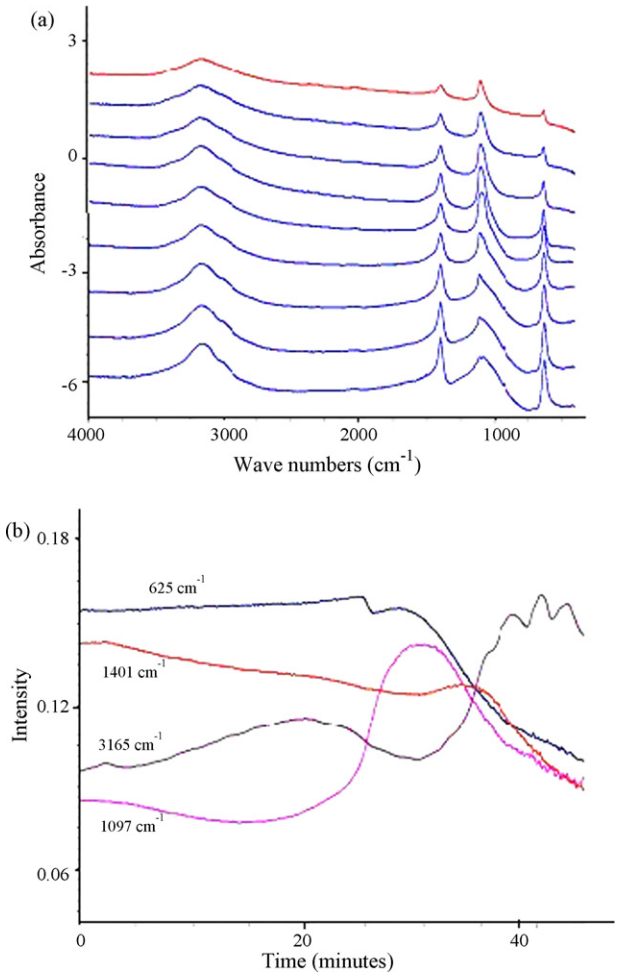

Fig. 9. (a) IR spectra and (b) IR characteristics absorption peak intensity of the condensed phase decomposition products of the CoZF nanocrystallites (1% by mass) with AP at various temperatures.

The catalytic effect of the ferrite nanocrystallites on ignition delay of AP was also investigated. It can also be seen from Table 4 and Fig. 6 that both ignition delay and the activation energy (E^*) for thermal ignition for pure AP is lowered by these catalysts. AP + CoZF mixture have lowest value for D_i and E^* whereas AP + NZF has highest value. Lower value of activation energy infers high catalytic activity of these ferrites with AP.

Fig. 8a and b showed IR spectra of pure and IR characteristic absorption peak intensity of the condensed phase decomposition products of pure AP at various temperatures. The spectrum exhibit enhanced intensity of νCl–O (1087 cm^{-1}) and the mode of ClO_4^- (625 cm^{-1}) with temperature. Up to 523 K, ν_{as} (N–H) 3179 cm^{-1} and (N–H) bending 1407 cm^{-1}, intensity decreases gradually but above

Table 4
Ignition delay (D_i), activation energy (E^*) for ignition and co-relation coefficient (r) of AP + MTTMF nanocrystallites

Sample	D_i (s)					E^* (kJ/mole)	r	ln$A$
	300 °C	310 °C	320 °C	330 °C	340 °C			
AP	150	137	119	101	85	42.02	0.9913	0.000762
AP + NZF	101	92	80	68	60	39.23	0.9952	0.000770
AP + CuCoF	93	88	75	65	56	38.42	0.9881	0.000777
AP + NCuF	96	90	78	67	57	39.00	0.9876	0.000785
AP + CuZF	92	85	74	65	55	37.82	0.9911	0.000760
AP + CoNF	89	86	76	66	54	36.77	0.9681	0.000770
AP + CoZF	85	83	73	65	52	35.68	0.9587	0.000775

Table 5
IR shifts of AP and AP with MTTMF nanocrystallites

Assignments (cm^{-1}) ↓	AP	AP + NZF	AP + CuCoF	AP + NCuF	AP + CuZF	AP + CoNF	AP + CoZF
(N–H) asymmetric stretching	3179	3142	3317	3177	3177	3184	3165
(N–H) bending	1407	1401	1401	1405	1405	1405	1401
Cl–O	1087	1089	1085	1074	1105	1109	1097
ClO_4^-	625	629	632	625	632	632	625

523 K, a marked decrease occurs. The ClO_4^- modes are the most temperature sensitive because of the increased rotational motion at higher temperature. These changes in both the cation and anion internal modes could be related to increased ion liberation as well as LTD decomposition. Addition of a catalyst to AP enhances the rate, of N–H bond heterolysis in NH_4^+ and, O–H bond making in $HClO_4$. Decomposition reactions of energetic materials often involve both bond-breaking and bond-forming steps. Approximately 1000 of reactions may be involved in the decomposition and combustion of AP [22,23], because of the four elements and the full range of oxidation states utilized by nitrogen and chlorine. The breaking of an N–H bond, then proton transfer from NH_4^+ to ClO_4^- to form an O–H bond leads to the formation of NH_3 and $HClO_4$ is a primary step in condense phases [8]

$$\underset{(I)}{NH_4^+ + ClO_4^-} = \underset{(II)}{NH_3{-}H{-}ClO_4} = \underset{(III)}{NH_3{-}HClO_4} = NH_3(a) + HClO_4(a)$$
$$= NH_3(g) + HClO_4(g)$$

Secondary reactions occur at higher temperature through complex competitive steps to produce gaseous products.

Fig. 9 shows a series of IR spectra taken for a mixture of AP and MTTMF. In fact, addition of a catalyst in AP could cause slight spectral changes (frequency shift, Table 5). The νClO_4^- (625 cm^{-1}) and νCl–O (1074 cm^{-1}) modes becomes narrower and resolvable at higher temperature indicating the catalyzed disruption of NH_4^+ and ClO_4^-. Thus, the spectrum pattern of AP in presence of all six catalysts is same and catalyzing.

However, the observed catalytic activities cannot be correlated to the size of the studied MTTMF nanocrystallites which have almost similar size. According to proton transfer mechanism [11], (I) corresponds to the pair of ions in AP lattice. Decomposition or sublimation starts with proton transfer from ammonium ion to perchlorate ion. At first, molecular complex (II) is formed; then it decomposes into NH_3 and $HClO_4$. The molecules of NH_3 and $HClO_4$ either react in an adsorbed layer on surface of AP or deadsorb and sublime interacting in the gas phase. It is known that the surface area of MTMMF nanocrystallites is large due to their very small size and there are many reactive sites over the surface. Thus during the second exothermic decomposition of AP, MTMMF nanocrystallites can adsorb the gaseous reactive molecules on their surface and catalyze the reactions.

4. Conclusions

MTTMF nanocrystallites were prepared by a co-precipitation method, characterized by XRD and BET equation. They have been used as catalysts in the thermolysis of AP. The catalytic activity was found to be in the following order:

CoZF > CoNF > CuF > CuCoF > NCuF > NZF

Acknowledgments

The authors are grateful to Head, Chemistry Department of D.D.U. Gorakhpur University for laboratory facility. Thanks are also due to financial assistants by CSIR for providing Emeritus Scientist to G. Singh and UGC-DSA fellowship to Shalini Dubey.

References

[1] D.H. Chen, X.R. He, Mater. Res. Bull. 36 (2001) 1369.
[2] B.L. Cushing, V.L. Kolesnichenko, C.J. ÓConnor, Chem. Rev. 104 (2004) 3893.
[3] M. Banerjee, N. Verma, R. Prasad, J. Mater. Sci. 42 (5) (2007) 1833.
[4] Y. Wang, J. Zhu, X. yang, L. Lu, X. Wang, Thermochim. Acta 437 (2005) 106.
[5] V.V. Boldyerv, Thermochim. Acta 443 (2006) 1–36.
[6] S.Dubey, P.F. Siril, Propell. Explos. Pyrot., in press (2008).
[7] H. Duan, X. Lin, G. Liu, L. Xu, F. Li, J. Mater. Proc. Technol. (2008).
[8] G. Singh, D.K. Pandey, J. Energ. Mater. 20 (2002) 223.
[9] C.L. Carnes, K.J. Klabunde, J. Mol, A Catal, Chem. 194 (2003) 227.
[10] G. Singh, S.P. Felix, Combust. Flame 132 (2003) 422.
[11] G. Singh, I.P.S. Kapoor, S Dubey, P.F. Siril, J. Sci. Con. Proc. 1 (2008) 7–14.
[12] A.S. Albuquerque, J.D. Ardisson, W.A. Macedo, J. Appl. Phys. 87 (2000) 4352.
[13] X. Liu, X. Wang, J. Zhang, X. Lu, L. Lu, Thermochim. Acta 342 (1999) 67.
[14] L.S. Birks, H. Fridman, J. Appl. Phys. 17 (1946) 687.
[15] G. Singh, R.R. Singh, Res. Ind. 23 (1978) 92.
[16] G. Singh, S.K. Vassudeva, I.P.S. Kapoor, Indian J. Technol. 29 (1991) 589.
[17] N. Semonov, Chem. Kinetics and Chain Reactions, Clarendon Press, Oxford, U.K., 1935 (Chapter 18).
[18] E.S. Freeman, S. Gordon, J. Phys. Chem. 960 (1956) 867.
[19] J. Zinn, R.N. Rogers, J. Phys. Chem. 66 (1962) 2646.
[20] L.L. Bircumshaw, B.H. Newmann, Proc. R. Soc.; A 227 (1954) 115.
[21] P.M.W. Jacobs, G.S. Parasone, Combust. Flame 13 (1969) 419.
[22] W.A. Rosser, S.H. Inami, Combust. Flame 12 (1968) 427.
[23] N.E. Ermolin, O.P. Korobeinichev, A.G. Tereshenk, V.M. Foomin, Combust. Explos. Shock Waves 18 (1982) 180–189.